CHARACTERIZATION OF POST-EARTHQUAKE CONSTRUCTION AND DEMOLITION WASTES BY HYPERSPECTRAL IMAGING

BONIFAZI G., TROTTA O., CAPOBIANCO G. and SERRANTI S.

Department of Chemical Engineering Materials & Environment, Sapienza – University of Rome, Italy, giuseppe.bonifazi@uniroma1.it

SUMMARY: Earthquakes create significant volumes of rubbles and waste (CDWs- Construction and Demolition Wastes), strongly impacting the environment and posing health risks. This paper investigates an automatic sensor-based approach finalized to identify and classify different post-disaster CDWs in order to be recycled as second raw material. The investigated CDWs were generated at Amatrice and Norcia areas (central Italy) in 2016 and 2017. The study presents a methodology based on a combination of two analytical techniques, HyperSpectral Imaging (HSI) in the SWIR range (1000-2500 nm) and X-ray fluorescence (XRF), in order to discriminate different samples compositions – e.g. Concretes, Roof Tiles, Bricks, as well as the recognition of contaminants – e.g. cement matrix on the surface of the samples. Results can represent an important starting point for further development of fully optical HSI based recognition CDWs procedures to be utilized both *off-line* (i.e. laboratory scale) and *on-line* (i.e. sorting level at industrial scale).

1. INTRODUCTION

Construction and demolition wastes, or CDWs, arise from construction sites and in the total or partial demolition of buildings and infrastructures. CDWs represents the largest waste worldwide at around 30 to 40%: 36% in the European Union, and close to 67% in the United States (Ruiz L. et al., 2020), and at present, in the EU over 800 million tonnes are produced every year (Eurostat, 2017). CDWs are composed of different quantities of concrete, cement, bricks, gypsum products, ceramic products (e.g. tiles), glass, asphalt, wood, but also some hazardous materials like asbestos, etc. . The presence of dust and the consequent fine powder inhalation, especially of asbestos, causes breathing problems and continuous exposure can lead to cancer (Olsen et al., 2011). Even though these hazardous materials are banned, they do exist in old buildings as well as in buildings that did not follow regulations at the time of construction (Ginga C.P. et al., 2020).

Natural disasters create enormous amounts of CDWs (Akhtar A. et al., 2018) through the destruction of buildings and infrastructure in a short time (EPA, 2008; FEMA, 2007). Therefore, CDWs management after a disaster is more difficult than ordinary CDWs management, due to its complexity and contamination with hazardous materials. Moreover, the disaster debris impacts not only on the environment but also on rescue and emergency services, on the provision of lifeline support and on the socio-economic recovery of the affected areas (Brown et al., 2011). Thus, the management of wastes created by disasters has become an increasingly important issue that needs to be correctly addressed when responding to a disaster (Thummarukudy, 2012).

The volume of waste, its assortment in terms of constituting materials and environmental health hazards, the areal extent of the waste, the community priorities, the existing and disaster-specific

regulations, all need to be assessed to determine the feasibility of disaster waste-recycling programmes (Brown and Milke, 2011). Hence, post-disaster CDWs management is one of the most crucial activities during the recovery period (Karunasena G. et al., 2013).

A correct approach needs to be developed to set up an automatic and non-destructive system able to classify and separate different materials, without human support, in order to use these products as secondary raw material. Research works have already highlight the great difficulty to separate CDWs constituents (Bonifazi G. and Serranti S., 2014; Bonifazi et al., 2015; Bonifazi et al., 2019; Serranti S. et al., 2015) due to the high variability in composition and characteristics.

The main aim of this study was to develop an automatic system able to identify and to classify different CDWs, in particular inert CDWs collected from the collapse of building generated by Amatrice earthquake (2016-2017). To that purpose, a classification method was applied, starting from XRF analysis of inert samples and the utilization of H*yperS*p*ectral* I*maging* (HSI), working in the Short-Wave InfraRed (SWIR) range (1000-2500 nm). The chemical maps obtained by XRF were compared with the acquired hyperspectral images in order to validate the results, obtained by optical sensing. The acquired HSI images were processed adopting chemometric techniques, in order to identify different type of class of materials, e.g. tile-Brick, and eventually contaminant. The proposed strategy can represent a valid and efficient method that can support a fast and reliable identification of material for the recycling and recovery of CDWs material.

2. MATERIALS AND METHOD

2.1. Materials

Seventy inert CDWs samples, collected in various cities and towns in the area of Amatrice (RT), hit by the earthquake in 2016-2017, were investigated. The samples are thus representative of construction waste material coming from a natural disaster. In particular, the CDWs samples are composed of fragments of Brick, Tile, Concrete, Perforated Brick, Stone, and Roof Tile.

The different samples have been identified and characterized by XRF and divided into datasets to build the HSI classification model. More in details, for the training datasets 9 particles of Concrete, 9 Stones, 9 Roof Tiles, 9 Perforated Bricks, 9 Tiles and 6 Bricks (Figure 1a) were selected. For the validation dataset, samples were divided into 4 samples of Concrete, 3 Stones, 3 Roof Tiles, 3 Perforated Bricks, 3 Tiles and 3 Bricks (Figure 1b).

a **b**

Figure 1. RGB colour images of the acquired Construction and Demolition Waste (CDWs) samples: calibration dataset (a) and validation dataset (b).

2.2. Methods

2.2.1 X-ray Fluorescence

The samples were analysed by Xray- fluorescence (XRF) to evaluate the chemical composition and element distribution. XRF analysis was obtained using a Bruker Tornado M4 equipped with an Rh tube, operating at 50 kV, 200 μA, with 25 μm spot obtained with poly-capillary optics. Mapping acquisition conditions are 10 ms/pixel and step size 100 μm in vacuum condition at 25 mBar.

2.2.2 Hyperspectral imaging analysis

The HyperSpectral images were acquired using the SISUChemaXLTM Chemical Imaging Workstation (Specim, Finland), equipped with an ImSpectorTM N25E imaging spectrograph (Specim, Finland) working in the short-wave infrared range (SWIR: 1000-2500 nm). The analytical station is controlled by a PC unit equipped with specialized acquisition/preprocessing software (ChemadaqTM), to handle the different units and the sensing device constituting the platform and perform the acquisition and the collection of spectra.

Samples were acquired with a macro lens of 15 mm and a field of view of 10 cm, and the spectral resolution was 6.3 nm. Calibration for black and white references was automatically performed. Spectral data were first analysed adopting the PLS_Toolbox (Eigenvector Research, Inc.) under Matlab® environment (The Mathworks, Inc.) to perform PCA and Statistics and Machine Learning Toolbox™ for kNN classification model.

The Principal Component Analysis (PCA) was applied for exploratory data analysis, to define classes and to perform the calibration dataset. Data were pre-processed in order to remove scattering and emphasize spectral variation. This techniques is a powerful and versatile method capable of providing an overview of complex multivariate data. PCA can be used for revealing relations between variables and relations between samples (e.g. clustering), detecting outliers, finding and quantifying patterns, generating new hypotheses as well as many other things (Bro and Smilde, 2014). It was used to decompose the "processed" spectral data into several principal components (PCs) (linear combinations of the original spectral data) embedding the spectral variations of each collected spectral data set. According to this approach, a reduced set of factors is produced. Such a set can be used for discrimination since it provides an accurate description of the entire dataset. Samples characterized by similar spectra, belonging to the same class of products, are grouped in the same region of the score plot related to the first two or three PCs, whereas samples characterized by different spectral features will be clustered in other parts of this space.

The Principal Component Analysis based k-Nearest Neighbor (PCA-kNN) method was applied for classification models. PCA-kNN classification is one of the most fundamental and simple algorithms used in classification methods, in particular, it is a powerful non-parametric classification system based on no prior knowledge about the data distribution (Parvin et al., 2008). KNN classification was developed from the need to perform discriminant analysis when reliable parametric estimates of probability densities are unknown or difficult to determine (Parvin et al., 2008). kNN classification algorithm tries to find the k nearest neighbours of a query vector and uses a majority vote to determine its class label, among the predefined classes. Without prior knowledge, the kNN classifier usually applies Euclidean distances as the distance metric. The performance of a kNN classifier is primarily determined by the choice of k and the applied distance metric (Imandoust & Bolandraftar, 2013). This number decides how many neighbours (where neighbours are defined by a distance metric) influence the classification. kNN classification approach has been widely used in various types of classification tasks. This classification approach has gained popularity due to its low implementation cost and a high degree of classification efficiency. However, its sample similarity computing is very large, which limits its applications in some cases characterized by high dimensional spaces or very large training sets (Du & Chen, 2013). In order to

reduce the computation time and memory requirement, without decreasing classification capability, the kNN algorithm was applied to the score matrix T computed by PCA model (Capobianco et al., 2017). Classification models were then evaluated using the following parameters: *Sensitivity* and *Specificity* in calibration (Cal) and cross-validated (CV):

Table 1. Results of mass percentage (%) of the major elements belonging to each class constituting the calibration dataset.

Class	Ca	Si	Fe	Al	K	Mg	Ti	Mn	S	Sr
Concrete	72.51	13.49	5.80	4.17	2.03	-	0.61	0.19	0.88	0.32
Brick	37.52	34.08	10.97	9.65	4.27	1.38	1.13	0.29	0.71	-
Aggregate/Stone	41.05	43.44	4.32	5.55	3.40	0.25	0.60	1.00	0.26	0.13
Perforated Brick	42.17	26.21	12.97	8.46	3.68	-	1.12	0.34	5.05	-
Roof tile	43.91	29.05	11.50	8.52	3.96	-	1.15	0.33	1.58	-
Tile	14.96	48.98	8.69	17.24	6.79	0.19	1.37	1.39	0.39	-

Sensitivity: TP/(TP + FN) (1)

Specificity: TN/(TN + FP) (2)

being TP the true positive and FN the false negatives. The best models are obtained when similar values are obtained for Sensitivity and Specificity in Cal and CV, thus demonstrating the robustness of the developed model (Kimuli D. et al., 2018).

3. RESULTS AND DISCUSSIONS

The investigated samples were first analysed, as previously outlined, by XRF and then according to the results divided into six classes generating a calibration and a validation dataset. For the calibration dataset were thus acquired six hyperspectral images representative of each group – e.g. Brick and tile, a mosaic procedure was then applied to obtain a single hypercube (Figure 2a). A single acquisition has been done for the validation dataset. In Table 1, the XRF average values of the different elements detected in the different individuals constituting the calibration set are reported.

Samples composed of concrete show a large amount of calcium in the cement matrix, represented by more than ~72 % of Ca, with a large and visible aggregate/stone immersed in the matrix, characterized by high porosity. In Figure 2b, the high presence of silicon or calcium in class aggregate/stone is due to calcite ($CaCO_3$) or flint (SiO_2), which are the most aggregate utilised in the construction sector. The cement matrix is also present on the surface of some samples as a contaminant. Tiles are mainly composed of silicon, aluminium and potassium (Figure 2c). This is because tiles are mainly composed of quartz and cristobalite, plus minor plagioclase and a variable amount of non-crystalline phases (Fiori C. et al., 1989). Brick samples show a matrix characterized by low porosity. A high presence of calcium, silicon, iron and aluminium is detected, moreover there is a high presence of magnesium compared to other classes. Finally, Perforated Bricks and Roof Tiles present similar composition in term of mass percentage, but with different distribution on the surface. Moreover, in perforated Brick a high presence of sulphur is detected. Hazardous minerals such as asbestos have not been detected.

An exploratory data analysis based on PCA was carried out. Different pre-processing methods have been adopted in order to highlight the spectral differences among samples. In particular, the following algorithms pre-processing chain was applied: *Smoothing*, *Multiplicative Scatter Correction* (MSC) (Median, no intercept), *Detrend, Mean Center* (MC). In Figures 3a and 3b, the average raw and pre-processed spectra of the analysed samples are reported. The absorption features, visible around 1400 nm and 1900 nm, in the spectra are due to the O-H stretching and H-

O-H bending vibrations in the water molecules (Crowley et al., 2003). Moreover, the absorption in aggregate spectra at 2350 nm could identify calcite which is one of the ingredients of cement in the

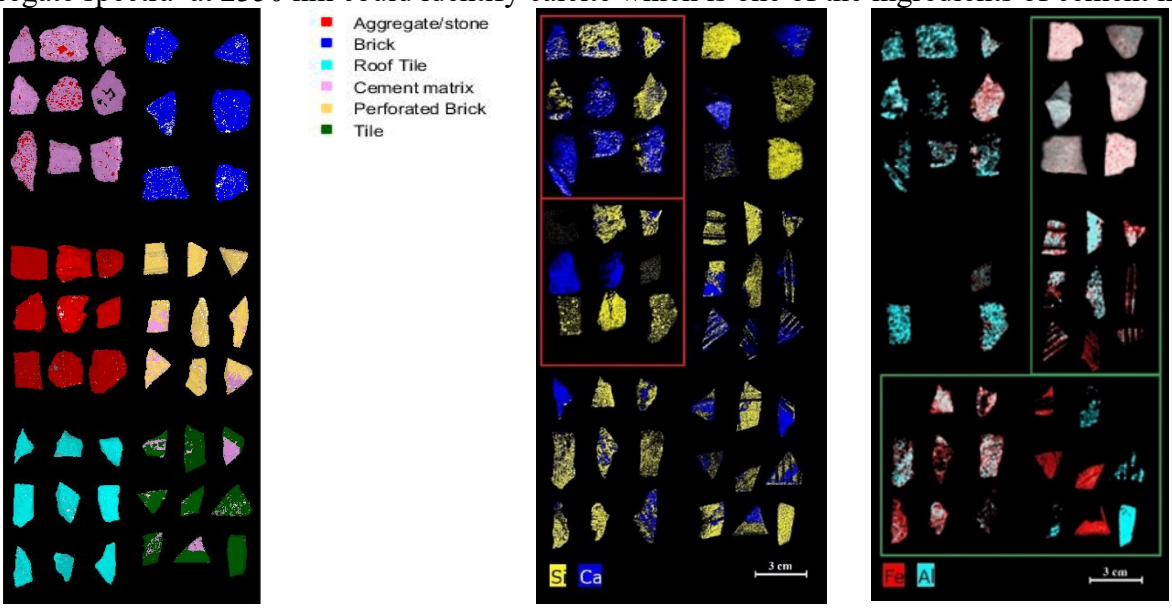

a **b** **c**

Figure 2. Calibration dataset, six classes have been defined inside the dataset (a), XRF results of calibration dataset, distribution of Si-Ca (b) and XRF map representative of Fe-Al (c).

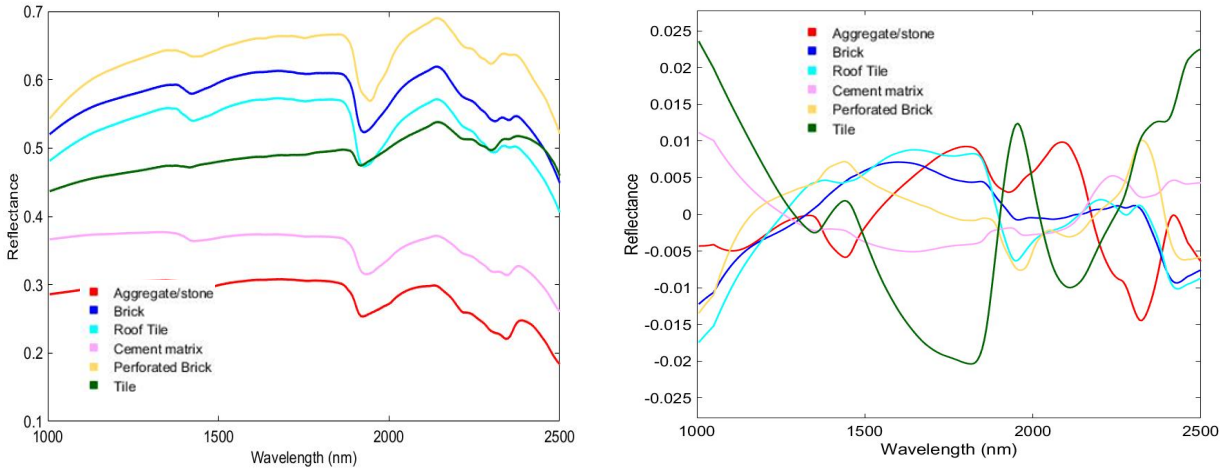

a **b**

Figure 3. SWIR average spectra of the different classes selected as results of PCA application to samples constituting the calibration dataset before (a) and after (b) pre-processing. Applied pre-processing sequence: *Smoothing*, MSC, *Detrend* and MC.

form of limestone and other forms of calcium carbonate (Goetz et al., 2009). Tile seems to have more accentuate absorption around 2200 nm, this characteristic could be attributed to a higher content of Al as observed by XRF map results. In fact, a combination band related to Al-O-H bond is detected in the SWIR range between 2180 nm and 2230 nm (Herrmann et al., 2001). After pre-processing, an exploratory data analysis based on PCA was carried out. PCA model requires 6 PC to express a total captured variance of 95.96% and shows a complex clusters scenario. The high variability is due to the heterogeneity and complexity of the dataset due to sample variability in terms of composition, morphologies and textures (e.g. different high and roughness of the surfaces).

Some spectral signatures show similar absorption. To improve the separation three score plots, better evidencing PCA differences (e.g. different clouds assessments), were analysed and reported in the following.

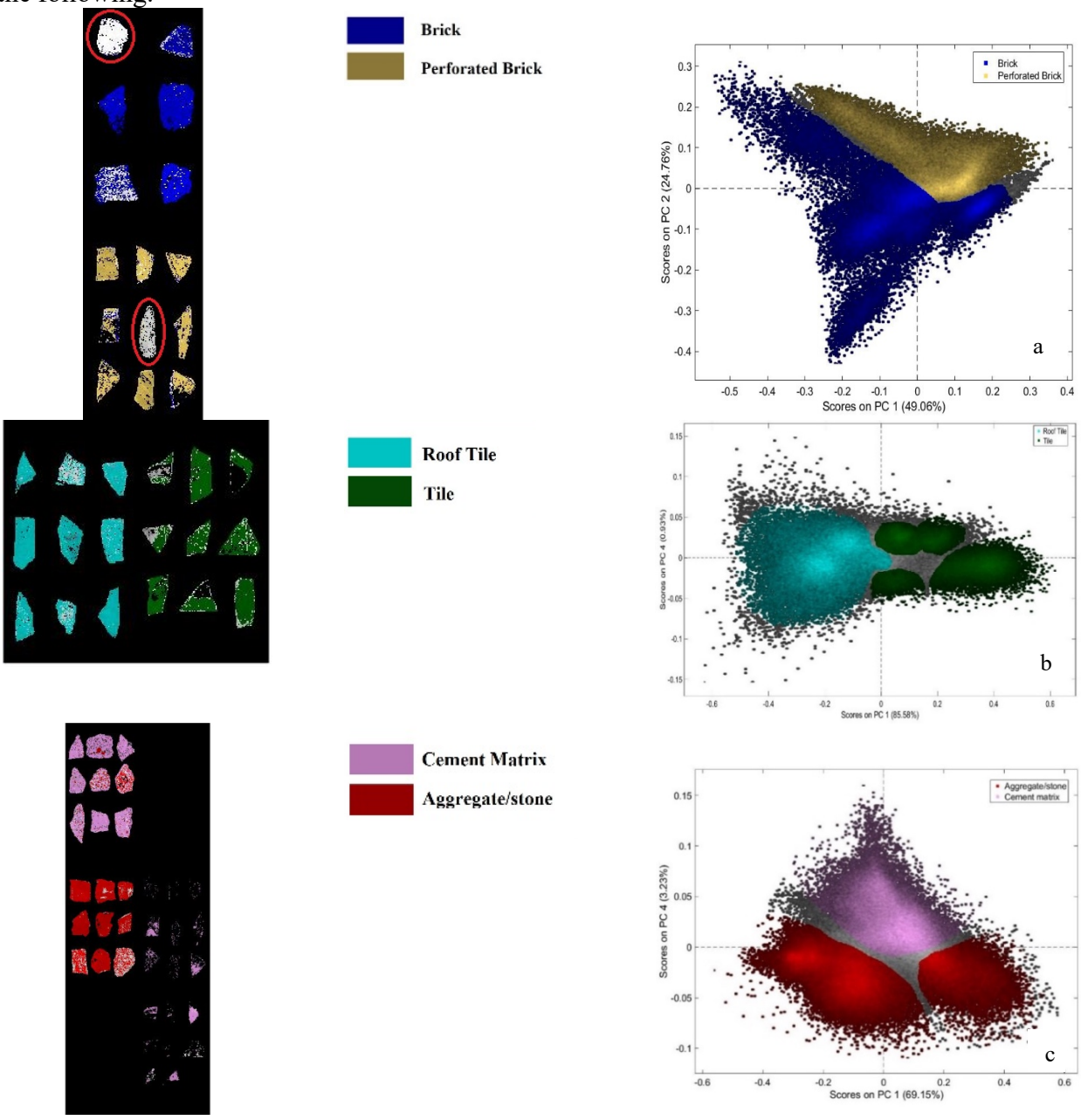

Figure 4. Calibration datasets and score plots: PC1-PC2 representative of classes Brick-Perforated Brick (a), PC1-PC4 representative of classes Roof Tile-Tile (b) and PC1-PC4 representative of classes Aggregate/Stone-Cement Matrix (c).

The first score plot (Figure 4a) does not realize a good discrimination between Bricks and perforated Bricks sample, due to samples fingerprints similarity, for this reason one sample of Brick and one of perforated Brick are not correctly recognised (i.e. individuals surrounded by red circles In Figure 4a). The analysis of the second score plot (Figure 4b), shows a high variability due to the different type of materials, in this case Roof Tiles and Tiles. The PC4 score plot shows seven cluster due to the relative variability. In detail, four groups represent Tile class characterized by high variance and three groups of Roof Tile. Finally, the third score plot (Figure 4c) shows the separation between Cement Matrix and Aggregate/stone classes. In particular, through PC4, the

Aggregate/stone is clustered in two groups, related respectively to aggregates high in silicon and high in calcium.

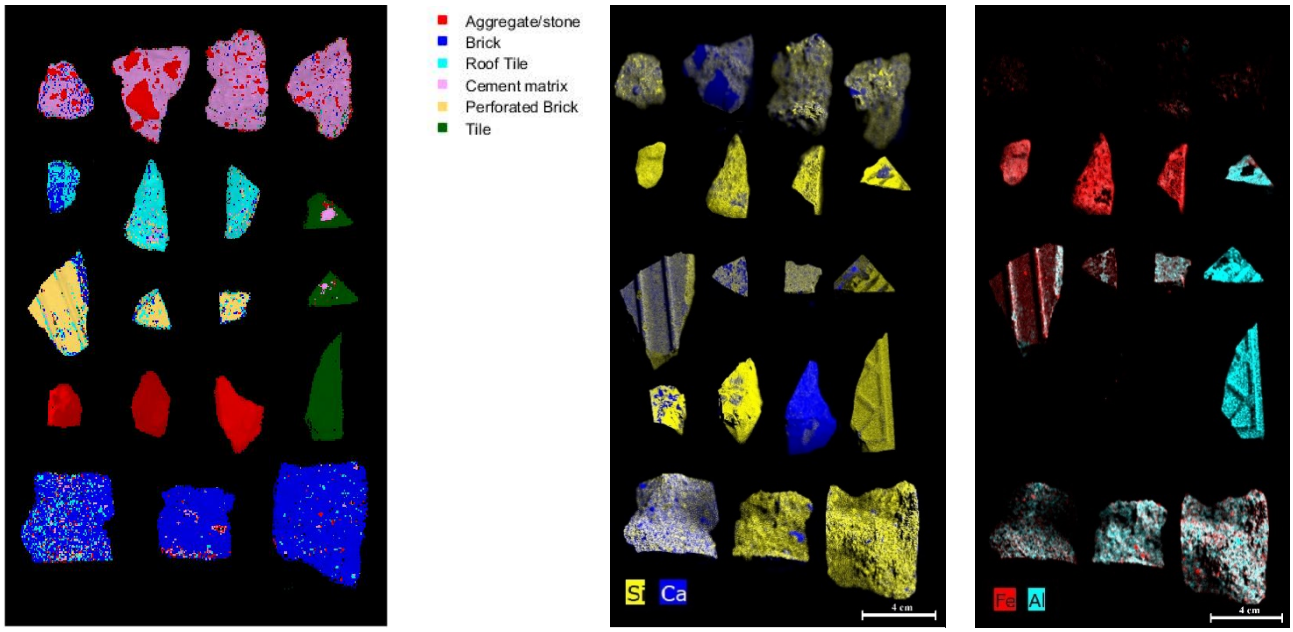

a **b** **c**

Figure 5. XRF map representative of Ca-Si (a), XRF map representative of Al-Si (b) and prediction maps obtained as result of PCA-kNN (c).

After PCA, the PCA kNN classifier was built and applied to the validation dataset. The result of the classification is reported, in term of a prediction map (Figure 5a). Results show as all the investigated classes are correctly identified and classified and in order to validate them the chemical maps obtained by XRF (Figures 5b and 5c) were compared with the prediction map obtained by optical sensing. Compositional and textural attributes, as investigated by XRF, confirm the variability detected by HSI device, evidencing the presence of common elements in all inert CDWs samples but with different distribution and concentration (Table 2). The model shows just a few misclassification errors for all six classes. The very few classification errors are always related to the morphology of the samples and the different high.

Table 2. Results of mass percentage (%) of the major elements belonging to each class in validation dataset.

Class	Ca	Si	Fe	Al	K	Mg	Ti	Mn	S	Sr
Concrete	79.66	10.42	3.71	3.15	1.03	0.44	0.39	0.17	0.83	0.20
Brick	37.76	33.82	10.8	9.14	4.21	2.51	1.03	0.23	0.34	0.16
Aggregate/Stone	53.27	45.17	0.68	-	0.34	-	0.17	0.11	0.26	-
Perforated Brick	34.95	29.28	13.34	9.58	4.59	-	1.27	0.41	6.35	0.23
Roof Tile	40.36	28.16	11.05	9.21	3.82	0.28	1.23	2.76	3.13	-
Tile	15.46	51.69	5.89	16.47	6.00	2.43	1.55	0.13	0.38	-

The results in terms of *Sensitivity* and *Specificity* (Table 3) confirm the good quality of the model, with values ranging from 0.82 to 1.00 and 0.81 to 1.00 respectively, both in calibration and cross-validation.

4. CONCLUSIONS

The study was carried out to investigate the combined utilization of X-ray fluorescence (XRF) and HyperSpectral Imaging (HIS) to perform a characterization of inert CDWs samples. A model was developed to evaluate the possibility to classify different inert CDWs with similar chemical composition and to recognize the presence of contaminant, e.g. the residue of cement matrix on the surface of the sample. Results showed that the proposed approach can be used for detection and characterization of inert CDWs, thus confirming the potentialities of the HSI method. Moreover, this approach represents a fast and non-destructive tool that can be utilized to develop and implement the waste management after a post-disaster. This method could be further implemented at the recycling plant level, in order to develop fully optical HSI based recognition CDWs procedures to be utilized both *off-line* (e.g. the analytical level at laboratory scale) and *on-line* (e.g. sorting level at industrial scale). Future developments will be addressed to increase performance for the identification of the different type of material in the same class in construction and demolition waste, e.g. ceramic tile to porcelain tile.

Table 3. *Sensitivity* and *Specificity* of calibration (Cal) and cross validation (CV) of the PCA-kNN model.

Class	*Sensitivity* (Cal)	*Specificity* (Cal)	*Sensitivity* (CV)	*Specificity* (CV)
Aggregate/stone	0.94	0.99	0.93	0.99
Background	0.97	1.00	0.97	1.00
Brick	0.89	0.98	0.89	0.98
Roof Tile	0.82	0.98	0.81	0.98
Cement matrix	0.90	0.97	0.89	0.97
Perforated Brick	0.88	0.99	0.88	0.99
Tile	0.89	0.99	0.89	0.99

REFERENCE

Akhtar A., Sarmah A.K. (2018) Construction and demolition waste generation and properties of recycled aggregate Concrete: A global perspective. *Journal of Cleaner Production*, 186, 262–281.

Bonifazi G. and Serranti S. (2014) Hyperspectral imaging applied to end-of life Concrete recycling, *Proc. SPIE* 9022, 90220V.

Bonifazi G., Capobianco G., Palmieri R., Serranti S. (2019) Hyperspectral imaging applied to the waste recycling sector. *Spectroscopy Europe,* Vol. 31, n. 2.

Bonifazi G., Palmieri R., Serranti S. (2015) Hyperspectral imaging applied to end-of-life (EOL) Concrete recycling, *Optical Characterization of Materials - conference proceedings*.

Bro R., Smilde A.K., Hubert M., Song X., Yu R., Holmberg M., Lundstrom I. (2014) Principal component analysis. *Analytical Methods*, 6, p. 2812.

Brown C., Mike M., Seville E. (2011) Disaster Waste management: A review of articles. *Waste Management* 31, 1085-1098.

Capobianco G., Bracciale M. P., Sali D., Sbardella F., Belloni P., Bonifazi G., Serranti S., Santarelli M.L., Guidi M. C. (2017) Chemometrics approach to FT-IR hyperspectral imaging analysis of degradation products in artwork cross-section. *Microchemical Journal*, 132, 69-76.

Crowley J.K., Williams D.E., Hammarstrom J.M., Piatak N., Chou I.M., Mars J.C. (2003) Spectral reflectance properties (0.4-2.5 lm) of secondary Fe-oxide, Fehydroxide, and Fe-sulphate-hydrate minerals associated with sulphide-bearing mine wastes. *Geochemistry: Exploration, Environment*, Analysis, 3, 219–228.

Du M. and Chen X. (2013) Accelerated k-nearest neighbors algorithm based on principal component analysis for text categorization. *Journal of Zhejiang University-SCIENCE*, 14, pp. 407-416.

Environmental Protection Agency (EPA) (2008) Planning for Natural Disaster Waste, available at: http://www.epa.gov/CDmaterials/pubs/pndd.pdf

Eurostat (2017) Generation of Waste-by-Waste Category, Hazardousness and NACE Rev 2 Activity. Access at URL: https://appsso.eurostat.ec.europa.eu/nui/show.do?dataset=env_wasgen&lang=en

Federal Emergency Management Agency (FEMA) (2007) Public Assistance: Waste Management Guide, available at: http://www.fema.gov/government/grant/pa/demagdes.html

Fiori C., Fabbri B., Donati G., Venturi I. (1989) Mineralogical composition of the clay bodies used in the Italian tile industry. *Applied Clay Science*, 4(5-6), 461–473.).

Ginga C. P., Ongpeng J. M. C., Daly M. K. D. (2020) Circular Economy on Construction and Demolition Waste: A Literature Review on Material Recovery and Production. *Materials*, 13, 2970.

Goetz A.F.H., Curtiss B., Shiley D.A. (2009) Rapid gangue mineral concentration measurement over conveyors by NIR reflectance spectroscopy. *Minerals Engineering*, 22, 490–499.

Herrmann W., Blake M., Doyle M., Huston D., Kamprad J., Merry N., Pontual S. (2001) Short wavelength infrared (SWIR) spectral analysis of hydrothermal alteration zones associated with base metal sulfide deposits at Rosebery and Western Tharsis, Tasmania, and Highway-Reward, Queensland. Econ. Geol. 96, 939–955

Imandoust S.B. and Bolandraftar M. (2013) Application of K-Nearest Neighbor (KNN) approach for predicting economic events: theoretical background. *International Journal of Engineering Research and Applications*, 3, 605-610.

Karunasena G., Rameezdeen R., Amarathunga D. (2013) Post-Disaster C&D Waste Management: The Case of COWAM Project in Sri Lanka. Paper presented at the *Australasian Journal of Construction Economics and Building-Conference Series.*

Kimuli D., Wang W., Jiang H., Zhao X., Chu X. (2018) Application of SWIR hyperspectral imaging and chemometrics for identification of aflatoxin B1 contaminated maize kernels. *Infrared Physics & Technology,* 89, 351–362.

Olsen N. J., Franklin P. J., Reid A., de Klerk N. H., Threlfall T. J., Shilkin K., Musk B. (2011). Increasing incidence of malignant mesothelioma after exposure to asbestos during home maintenance and renovation. *Medical Journal of Australia,* 195(5), 271-274.

Palmieri R., Bonifazi G., Serranti S., (2013) Automatic detection and classification of eol-Concrete and resulting recovered products by hyperspectral imaging, *Proc. SPIE*, *9106*, Baltimore, USA.

Parvin H., Alizadeh H., Minaei-Bidgoli B. (2008) MKNN: modified k-nearest neighbor, S.I. Ao, Douglas G., Grundfest W.S., Schruben L., Burgstone J. (Eds.), *Proc. World Congress on Engineering and Computer Science (WCECS 2008)*, Newswood Limited, San Francisco, 831-834.

Ruiz L., Ramón X., Domingo S. (2020) The circular economy in the construction and demolition waste sector- A review and an integrative model approach. *Journal of Cleaner Production*, 248, 119238.

Serranti S., Palmieri R., Bonifazi G. (2015) Hyperspectral imaging applied to demolition waste recycling: an innovative approach for quality control. *Journal of Electronic Imaging*, 24, 043003.

Thummarukudy M. (2012) Disaster waste Management: An overview, in Shaw, R. and Tran, P. (eds.), Environment disaster linkages, Emerald Group Publishing limited.

Wise B. M., Gallagher N. B., Bro R. (2007) Chemiometric Tutorial for PLS_Toolbox and Solo. Eigenvector Reserarc, Inc., 3905 West Eaglerock Drive, Wenatchee, Washington.